THE JOURNAL OF BIOLOGICAL CHEMISTRY VOL. 287, NO. 35, pp. 29237–29249, August 24, 2012

Conformational Changes in Inositol 1,3,4,5,6-Pentakisphosphate 2-Kinase upon Substrate Binding

*ROLE OF N-TERMINAL LOBE AND ENANTIOMERIC SUBSTRATE PREFERENCE**

Received for publication, March 22, 2012, and in revised form, June 25, 2012 Published, JBC Papers in Press, June 28, 2012, DOI 10.1074/jbc.M112.363671

José Ignacio Baños-Sanz[‡1], Julia Sanz-Aparicio[‡], Hayley Whitfield[§2], Chris Hamilton[¶], Charles A. Brearley[§3], and Beatriz González [‡4]

From the [‡]Departamento de Cristalografía y Biología Estructural, Instituto de Química-Física "Rocasolano," CSIC, Serrano 119, 28006-Madrid, Spain and the [§]School of Biological Sciences and [¶]School of Pharmacy, University of East Anglia, Norwich Research Park, Norwich NR4 7TJ, United Kingdom

Background: IP_5 2-K is essential for higher inositide metabolism and signaling.
Results: Crystal structures and biochemical data reveal different IP_5 2-K conformational states.
Conclusion: IP_5 2-K undergoes conformational changes upon nucleotide and inositide binding, with the N-lobe being essential for substrate recognition and IP_4 enantiomer selection.
Significance: Understanding the determinants of enzyme function and substrate specificity will enable rational design of inhibitors.

Inositol 1,3,4,5,6-pentakisphosphate 2-kinase (IP_5 2-K) catalyzes the synthesis of inositol 1,2,3,4,5,6-hexakisphosphate from ATP and IP_5. Inositol 1,2,3,4,5,6-hexakisphosphate is implicated in crucial processes such as mRNA export, DNA editing, and phosphorus storage in plants. We previously solved the first structure of an IP_5 2-K, which shed light on aspects of substrate recognition. However, failure of IP_5 2-K to crystallize in the absence of inositide prompted us to study putative conformational changes upon substrate binding. We have made mutations to residues on a region of the protein that produces a clasp over the active site. A W129A mutant allowed us to capture IP_5 2-K in its different conformations by crystallography. Thus, the IP_5 2-K apo-form structure displays an open conformation, whereas the nucleotide-bound form shows a half-closed conformation, in contrast to the inositide-bound form obtained previously in a closed conformation. Both nucleotide and inositide binding produce large conformational changes that can be understood as two rigid domain movements, although local changes were also observed. Changes in intrinsic fluorescence upon nucleotide and inositide binding are in agreement with the crystallographic findings. Our work suggests that the clasp might be involved in enzyme kinetics, with the N-terminal lobe being essential for inositide binding and subsequent conformational changes. We also show how IP_5 2-K discriminates between inositol 1,3,4,5-tetrakisphosphate and 3,4,5,6-tetrakisphosphate enantiomers and that substrate preference can be manipulated by Arg^{130} mutation. Altogether, these results provide a framework for rational design of specific inhibitors with potential applications as biological tools for *in vivo* studies, which could assist in the identification of novel roles for IP_5 2-K in mammals.

Inositol phosphates (IPs,[5] inositides) are a group of molecules with diverse roles in cell signaling (1). They present crucial roles in DNA reparation and editing, endocytosis, vesicle trafficking, ionic channel regulation, and control of telomere length (2). There are at least 30 different IPs in mammal cells, and their metabolism is dominated by receptor-coupled activation of phospholipase C, which cleaves phosphatidylinositol 4,5-bisphosphate to produce diacylglycerol and inositol 1,4,5-trisphosphate (IP_3), a starting point for the synthesis of many IPs (2). The levels of these molecules are regulated by families of inositol phosphate kinases or phosphatases that phosphorylate/dephosphorylate the different positions of the inositol ring.

This work is focused on the study of one of those kinases, the inositol 1,3,4,5,6-pentakisphosphate 2-kinase (IP_5 2-K, IPK1), an enzyme that catalyzes the synthesis of a crucial compound, inositol 1,2,3,4,5,6-hexakisphosphate (IP_6), by phosphorylation of the axial 2-OH of IP_5. IP_5 2-K has been cloned and characterized from many organisms, from yeast to humans (3–8). *Ipk1* gene disruption in mice results in early lethality of the embryos (9). IP_6 participates in mRNA export (10), regulation of chromatin state (11), developmental processes (12), and apo-

* This work was supported in part by Grants BFU200-02897/BMC and BFU2011-24982 from the Ministerio de Ciencia e Innovación.

The atomic coordinates and structure factors (codes 4axc, 4axd, 4axe, and 4axf) have been deposited in the Protein Data Bank, Research Collaboratory for Structural Bioinformatics, Rutgers University, New Brunswick, NJ (http://www.rcsb.org/).

[1] Supported by Formación de Profesorado Universitario Fellowship AP2008-00916 from the Ministerio de Educación.
[2] Supported by a Dean's studentship from the Faculty of Science, University of East Anglia.

[3] To whom correspondence may be addressed. E-mail: c.brearley@uea.ac.uk.
[4] To whom correspondence may be addressed. Tel.: 34-91-5619400; Fax: 34-91-564-24-31; E-mail: xbeatriz@iqfr.csic.es.

[5] The abbreviations used are: IP, inositol phosphate; *At*, *A. thaliana*; IP_5 2-K, inositol 1,3,4,5,6-pentakisphosphate 2-kinase; IP_6, inositol 1,2,3,4,5,6-hexakisphosphate; IPK, inositol polyphosphate kinase; IP_3, inositol 1,4,5-trisphosphate, IPmK, inositol polyphosphate multikinase; IP_4 or Ins-(1,4,5,6)-P_4, inositol 1,3,4,5-tetrakisphosphate; Ins(3,4,5,6)P_4, inositol 3,4,5,6-tetrakisphosphate; Ins(1,3,4,5,6)P_5, inositol 1,3,4,5,6-pentakisphosphate; AMPPNP, adenosine 5′-(β,γ-imido)triphosphate; r.m.s.d., root mean square deviation.

ptosis (13). In addition, IP_6 serves as substrate for the synthesis of diphosphoinositol polyphosphates (inositol pyrophosphates), emergent molecules with multiple functions (14). In plants, IP_6 has been shown to be involved in the maintenance of basal resistance to plant pathogens (15) and represents a reserve of phosphorus in storage tissues. The high phosphorus content of seeds is a cause of major problems for both human health and the environment (16). In developing countries, grain-based diets provide an excess of IP_6, which exacerbate iron and zinc malnutrition due to the potent metal-chelating properties of IP_6. In addition, monogastric animals are unable to digest IP_6, thus excreting it which leads to water eutrophication (17). Consequently, there is a high demand for the development of low phytate seeds (18–20).

IP_5 2-K belongs to the inositol polyphosphate kinases (IPKs) family, which comprises three other subfamilies as follows: IP_3 3-kinases, IP multikinases (IPmKs), and IP_6 kinases (2). The first structure of an IPK, the IP_3 3-K isoform A (21, 22), became available in 2004 and was followed by the structure of yeast IPmK (23). More recently, we reported the first structure of an IP_5 2-kinase (24) from *Arabidopsis thaliana,* which showed, unexpectedly, that this enzyme belongs to the IPK family, albeit the most distant member. IP_5 2-Ks, as well as other IPKs, conserve key features with protein kinases (PKs); they fold in two lobes (N- and C-lobes), connected by a hinge, and the N-terminal lobe core conserves an $\alpha+\beta$ fold. In addition, the essential features of ATP recognition between both lobes are conserved. However, the C-lobe of IPKs is not conserved with PKs, and the inositide-binding site, located in a separated portion of this C-lobe, is characteristic for each enzyme within the IPK family. In particular, IP_5 2-K shows the most divergent region for inositide binding (referred to as C_{IP}-lobe) that is formed by multiple α-helixes folded into a unique large domain that encompasses almost half of the protein (24). There is a different family of inositol phosphate kinases, exemplified by the *Entamoeba histolytica* enzyme (25), that show the ATP-grasp fold. The most recent addition to this family is the diphosphoinositol pentakisphosphate kinase subfamily, the structure of which was recently solved (26). Although these enzymes display a different fold from IPKs, both share some essential features of catalysis (26). Representatives of all the inositol phosphate kinases mentioned, except IP_6 Ks, have been crystallized and many of them in presence of substrates or products, yielding complete or partial clues about their catalytic mechanism.

The structural analysis of IP_5 2-K offers a better understanding of its function at the molecular level. The reported complexes of IP_5 2-K with inositide, both substrate (IP_5) and product (IP_6), and the ternary complexes with substrates (IP_5/AMPPNP) and products (IP_6/ADP) allowed us to identify key residues defining inositide- and nucleotide-binding sites, as well as crucial elements in the enzymatic mechanism (24). However, there are several aspects that remain to be understood. In particular, all the complexes display a common conformation of the active site that does not correlate with different changes observed in the fluorescence spectra upon substrate binding. We attributed these changes to putative conformational changes that could not be fully characterized because the inositide presence was a requirement for the crystallization of *At*IP_5 2-K samples (24, 27); consequently, its apoform remained elusive. In this work, we have followed a strategy for growing crystals from IP_5 2-K in its free state that was also applied to obtain complexes with nucleotide, always in absence of inositide. The results provide a complete picture of the conformational changes produced upon inositide and/or nucleotide binding that allowed full identification of the molecular landmarks responsible for IP_5 2-K function. In agreement with the structural studies, fluorescence analysis shows significant IP_5 2-K changes upon substrate binding. In addition, the exact role of the IP_5 2-K N-lobe in protein conformational changes and substrate specificity has been also investigated. For this purpose, we have explored discrimination between enantiomers of two IP_4s, Ins(1,4,5,6)P_4 and Ins(3,4,5,6)P_4,[6] that have been reported to be substrates of plant IP_5 2-K *in vitro*, and we solved the structure of IP_5 2-K in ternary complex with ATP analog and Ins(3,4,5,6)P_4. Intriguingly, despite the wealth of literature on Ins(1,4,5,6)P_4 metabolism in yeasts and Ins(1,4,5,6)P_4/Ins(3,4,5,6)P_4 metabolism in animals, neither of these two isomers are considered physiological substrates of IP_5 2-K enzymes in these kingdoms. Our experiments provide a structural basis for such consideration.

The results presented here, together with our previous work, represent the first structural description of a complete catalytic cycle of IP_5 2-K enzymes and gives insights into the discrimination of enantiomeric substrates in IP_5 2-K.

EXPERIMENTAL PROCEDURES

Purification, Crystallization, and Data Collection—Wild type and W129A IP_5 2-K mutant were produced in *Escherichia coli* Rosetta (DE3) pLysS strain and purified as reported previously (28). The crystallization of W129A-IP_5 2-K mutant, in its apo- and AMPPNP-bound forms is detailed in Baños-Sanz *et al.* (28). Briefly, to obtain the W129A IP_5-2K crystals, equal amounts of protein solution (10 mg/ml) and precipitant (29% w/v PEG4000, 0.2 M $LiSO_4$, and 0.1 M Tris/HCl, pH 8.5) were mixed and equilibrated against a reservoir containing 0.5 ml of precipitant using the sitting drop technique. Seeding was used to obtain high quality crystals. Crystals appeared in 5 days at 18 °C. For data collection, crystals were cryoprotected using a gradual increase in the PEG content from 29 to 35% of the crystal mother liquor. For AMPPNP-bound IP_5 2-K, the mutated protein was mixed with 2 mM AMPPNP, and crystals were obtained in 0.5 M $(NH_4)_2SO_4$, 0.1 M sodium citrate tribasic, pH 5.6, and 0.8 M Li_2SO_4 and cryo-protected with this condition plus 20% glycerol. Seeding was again crucial to facilitate crystal growth. The ADP-bound IP_5 2-K crystals were obtained in the same condition, except the protein was incubated previous to crystallization trials with 2 mM ADP. To obtain wild type crystals in complex with Ins(3,4,5,6)P_4 and AMPPNP, we have followed our protocol previously reported (27). In this case, protein was incubated with 1 mM IP_4 plus 2 mM AMPPNP, crystallized, and cryoprotected under the same

[6] The following nomenclature is used: stereoisomers and enantiomers of inositol phosphates are numbered according to the D-assignment, thus D- and L-Ins(1,4,5,6)P_4 are identified as Ins(1,4,5,6)P_4 and Ins(3,4,5,6)P_4, respectively.

TABLE 1

Crystal data collection, structure determination, and refinement

Data for the outermost shell are given in parentheses. a.u. means asymmetric units.

Crystal	W129A	W129A/AMPPNP	W129A/ADP	IP$_5$ 2-K/AMPPNP/IP$_4$
Data collection				
Space group	$P2_12_12$	$P2_12_12$	$P2_12_12$	$P2_12_12_1$
Cell	66.00	63.06	63.72	61.62
	68.23	71.80	71.92	65.08
	105.80	100.23	100.62	122.49
Wavelength	0.9794 Å	1.0053 Å	0.9334 Å	0.9334 Å
Resolution range	47.44 to 2.25 Å	53.37 to 2.05 Å	39.49 to 2.50 Å	57.47 to 2.93 Å
*R*pim[a]	0.028 (0.180)	0.04 (0.158)	0.054 (0.204)	0.059 (0.161)
*R*merge[b]	0.072 (0.517)	0.098 (0.398)	0.105 (0.407)	0.146 (0.394)
Unique reflections	24,181 (3488)	29,280 (4191)	16,575 (2370)	77,497 (10881)
Redundancy	7.3 (7.4)	7.1 (7.3)	4.6 (4.8)	7.0 (6.9)
Completeness	99.6% (100%)	100% (100%)	99.8% (100.0%)	100.0% (100.0%)
Mean ($I/\sigma I$)	15.4 (3.8)	15.0 (4.9)	10.1 (3.6)	13.4 (4.9)
$I/\sigma(I)$	6.1 (1.5)	5.5 (1.9)	5.4 (1.9)	4.9 (1.9)
Wilson *B* value	47.4 Å^2	22.0 Å^2	39.7 Å^2	39.2 Å^2
Refinement statistics				
Molecules per a.u.	1	1	1	1
Resolution range	47.44 to 2.25 Å	53.37 to 2.05 Å	39.49 to 2.50 Å	57.47 to 2.93 Å
*R*factor[c]	0.24%	0.20%	0.22%	0.22%
*R*free	0.28%	0.25%	0.28%	0.28%
Protein atoms (non-H)	3151	3458	3391	3260
Ligand atoms (non-H) IP_4, IP_6, AMPPNP, ADP	0	31	27	59
Ions SO_4^{2-}, Zn^{2+}	21	26	31	1
Waters	74	324	66	0
r.m.s.d.				
Bonds	0.009 Å	0.008 Å	0.005 Å	0.005 Å
Angles	1.69°	1.69°	1.04°	1.06°
Mean *B* value				
Protein	59.27 Å^2	24.15 Å^2	41.10 Å^2	29.05 Å^2
Ligands	NA[d]	19.10	32.15	18.34
Waters	30.79	30.45	32.07	NA
Missing residues	1–2, 47–60, 152–161, 334–341, 382–387, 434–451	386, 434–451	158,159, 334–336, 386, 434–451	47–58, 155–158, 378–386, 437–451
Ramachandran data				
Most favored	92.5%	91.2%	92.4%	92.3%
Disallowed	0.3%	0.5%	0.3%	0.3%

[a] $R\text{pim} = \Sigma(1/(N-1))^{1/2}\,\Sigma|I(h)i - \langle I(h)\rangle|/\Sigma\Sigma\,\langle I(h)\rangle$.

[b] $R\text{merge} = 100\,\Sigma h\Sigma i|Ih, i - \langle Ih\rangle|/\Sigma h\Sigma iIh, i$, where the outer sum ($h$) is over the unique reflections and the inner sum (i) is over the set of independent observations of each unique reflection.

[c] $R\text{-factor} = \Sigma\,(|F_{obs} - F_{calc}|/\Sigma|F_{obs}|$ (*R*free is equivalent to *R*-factor for a randomly selected 5% subset of reflections not used in structure refinement).

[d] NA means not applicable.

conditions as for the other wild type crystal complexes (24). Diffraction data for all the crystals was collected using synchrotron radiation from European Synchrotron Radiation Facility (Grenoble, France). All the data were processed using iMosflm (29) and merged with Scala (30) from the CCP4 package (31). A summary of data collection statistics is shown in Table 1.

Structure Solution and Refinement—All the structures were solved by Molecular Replacement with Phaser program (32), using as a search model our previous wild type structure (Protein Data Bank code 2xan) (24) and dividing the model in two ensembles for the W129A mutant structures, as detailed previously (28). Several rounds of refinement with Refmac5 (33) were alternated with model building with the program Coot (34). Final refinement parameters are reported in Table 1. In particular, the electron density maps of the W129A-IP$_5$ 2-K crystal did not allow building of regions consisting of residues 46–59 in hinge 1 and part of hinge 3, whereas the W129A-IP$_5$ 2-K-nucleotide complex density maps allowed almost complete building of the model. The average *B*-factors of both crystals show significant differences, which is coherent with a high flexibility in the open form of the free enzyme, and the stabilization exerted by AMPPNP binding. The ADP-bound crystals present higher *B*-factors, revealing the importance of Pγ in the stabilization. Stereochemistry of the model was checked using PROCHECK (35). Protein pictures were performed with PyMOL (36). Protein motion along IP$_5$ 2-K different states has been analyzed manually and automatically using DymDOM server (37).

Mutant Production and Purification—The mutants was performed using the QuikChange protocol, employing the following pairs of oligonucleotides: 5′-GATTCGTATACAGAAGGCTGCGAGGAATGATAAAGCAATC-3′ and 5′-GATTGCTTTATCATTCCTCGCAGCCTTCTGTATACGAATC-3′ for R45A mutation; 5′-CGTCCGCTAGCGCGTGTTAATGC-3′ and 5′-GCATTAACACGCGCTAGCGGACG-3′ for W129A mutation; 5′-CGTCCGCTAGTGGCTGTTAATGC-3′ and 5′-GCATTAACAGCCACTAGCGGACG-3′ for W129V/R130A mutation; 5′-CGTCCGCTATGGGCTGTTAATGC-3′ and 5′-GCAGGCGATACCGCACAATTACG-3′ for R130A mutation; and 5′-CCCGGTGCTACCACCCCCTAATATGAGAGAACC-3′ and 5′-GGGGGTGGTAGCACCGGGAGAACCAGCCCC-3′ for ΔS253/ΔE255 deletions. Previous construction of wild type fused to lectin from *Letiporus sulphureus* was used as template (24). The incorporation of the mutations was assessed by DNA sequencing. Mutants were grown in *E. coli*

Rosetta (DE3) pLysS strain as wild type protein. Cell pellets were resuspended in buffer A (20 mM Tris, pH 8.0, 150 mM NaCl, 2 mM DTT plus a Complete EDTA free protease inhibitor mixture (Roche Applied Science)) and disrupted with a French press. The filtrated cell lysate was applied onto a Sepharose CL-4B column equilibrated previously with buffer A, and the protein was eluted with buffer A plus 200 mM lactose. Protein-containing fractions were pooled and diluted 3-fold with 20 mM Tris, pH 8, to reduce the salt concentration, loaded onto a heparin column, washed with buffer B (20 mM Tris, pH 8, 50 mM NaCl, 2 mM DTT), and eluted with a gradient between buffer B and C (20 mM Tris, pH 8, 1 M NaCl, 2 mM DTT). The eluted fused protein was cleaved by tobacco etch virus protease (protease/protein mass ratio 1:80), shaking the sample gently at 4 °C overnight. To remove the lectin of *L. sulphureus* tag, we used another Sepharose CL-4B column. Mutants were concentrated between 0.5 and 1 mg/ml and stored at −80 °C until use.

Enzyme Assays—Kinase assays were performed in 0.2-ml volumes on a Molecular Devices SpectraMax M5 Plate reader using an assay similar to that described previously (38, 39). The assay mixture contained 20 mM Hepes, pH 7.5, 1 mM $MgCl_2$, 0.1 mM ATP, 2 mM P-enolpyruvate, 0.15 mM NADH and 7.5 units ml^{-1} lactate dehydrogenase, 15 units ml^{-1} PK, 5 μM inositol phosphate. Reactions were started by addition of the above assay mixture to enzyme and 100 or 500 ng of native protein or mutant as specified in the text. Assays were run for 15 min at 25 °C and initial linear rate measurements (ΔOD min^{-1}) were determined using the SoftMax Pro software of the plate reader: initial rates were linear for 3–9 min. Assays were typically performed with 4–5 replicate wells and were repeated no less than three times.

Kinetic Analysis of Native and W129A Mutant—Kinase assays were performed with 100 ng of native or W129A protein and 0.3–10 μM Ins(1,3,4,5,6)P_5. Assays were performed with 4–5 replicate wells and repeated three times. $K_{m,\,app}$ and $V_{max,\,app}$ values were determined by nonlinear least squares regression of a plot of V_{app} *versus* substrate concentration fitted to the Michaelis-Menten equation in GraFit Version 5 (Erithacus Software Ltd.).

Fluorescence Assays—Substrate binding to native and W129A protein was followed at 25 °C by monitoring changes in intrinsic fluorescence recorded with an excitation wavelength of 295 nm, bandwidth 5 nm, and emission from 310 to 380 nm, bandwidth 10 nm, on a Cary Eclipse fluorescence spectrometer. The photomultiplier voltage was set to 800 V. Protein (14.5 μg) was suspended in 1 ml of 20 mM Hepes, pH 7.5, 1 mM $MgCl_2$ in a 10 × 3-mm cuvette. Inositol 1,3,4,5,6-pentakisphosphate or AMPPNP was added from 0.1 and 5 mM stocks, respectively. The total volume of ligand added was less than 1% of the sample volume. Data were exported in GraFit Version 5 (Erithacus Software Ltd.). Plots of fractional change in fluorescence ($F_o - F$)/F_o *versus* ligand concentration, determined at 335 nm) were analyzed by nonlinear least squares regression to a single site binding model in GraFit Version 5. Experiments were repeated three times.

RESULTS

Structure of IP_5 2-K Apo-form Represents the Open Conformation—Previously reported IP_5 2-K inositide-bound structures, with or without bound nucleotide, show a common conformation that leaves a hollow for ATP binding formed between the N-lobe and C-lobe. The inositide is mainly bound to the C-lobe (at the unique region named C_{IP}-lobe), but it also binds to a few N-lobe residues bringing together both lobes (Fig. 1*A*). We will refer to this state as "closed" or "inositide-bound" form. In this form, the β- and γ- phosphates of the ATP are linked to the G-loop (Glu^{18}–Asn^{21}), a feature common to PKs, and the active site is enclosed by residues from the structural elements α6 (Leu^{128}–Ala^{133}) and L3 (Gly^{251}–Ser^{261}) that interact forming a kind of clasp (Fig. 1*A, zoom*). Because the clasp seems to preclude the nucleotide from entering/leaving the active site, we suspected that the clasp elements might be unconnected in a putative open conformation, and therefore, we expected that L3 would present high mobility. Accordingly, the IP_5 2-K·IP_5 crystal complex showed some disorder at L3 (Protein Data Bank code 2xao). Moreover, *At*IP_5 2-K exhibits changes in gel filtration elution profile (data not shown) and in tryptophan intrinsic fluorescence (see below) upon substrate binding, indicative of structural changes, which in turn could arise from changes in the environment of Trp^{129}. We have therefore undertaken an in-depth study of the clasp role through characterization of several IP_5 2-K mutants (W129A, W129V/R130A, R130A, and ΔS253/ΔE255) (Table 2). One of these fully active mutants, W129A, allowed us to obtain crystals from the enzyme in its apo-form, *i.e.* in its unbound state. The crystals obtained present a different unit cell, space group, and crystal packing than the inositide-bound structures (Table 1) (28).

The W129A IP_5 2-K structure shows a similar overall fold to that reported previously for the enzyme, but the N-lobe and C-lobe are farther apart from each other forming a more open cleft (Fig. 1*B*). We will refer to this form as "open form" or "apo-form." Superposition of Cαs from open and closed (24) conformations gives an r.m.s.d. of 2.50 Å; however, a close inspection reveals that there is a significant motion of two independent portions of the protein (Fig. 1*C*) as follows: one is formed by most of the N-lobe, which includes residues 6–42 and 103–148 (r.m.s.d. of 1.27 Å superposing 81 residues from each state); and the other is composed of a segment of the N-lobe previously referred to as N-I (24) that includes residues 63–102, and the whole C-lobe (r.m.s.d. of 0.87 Å for 302 residues). This motion upon substrate binding can be described as an 18.4° rotation of one portion of the enzyme, which pivots about three regions of the polypeptidic chain acting as hinges; two of them are the two segments that connect N-I to the remaining part of the N-lobe (hinge 1, 42–63; hinge 2, 102–103) and the third one is the linker between N- and C-lobe (hinge 3: 148–159), a typical hinge common to the family of PKs (Fig. 1*C*). As expected, these hinges are the most disordered parts in the electron density reflecting its intrinsic flexibility. Apart from this general rigid-body movement, local changes occur particularly at α6 and L3 segments (Fig. 1*C,* and *bottom*

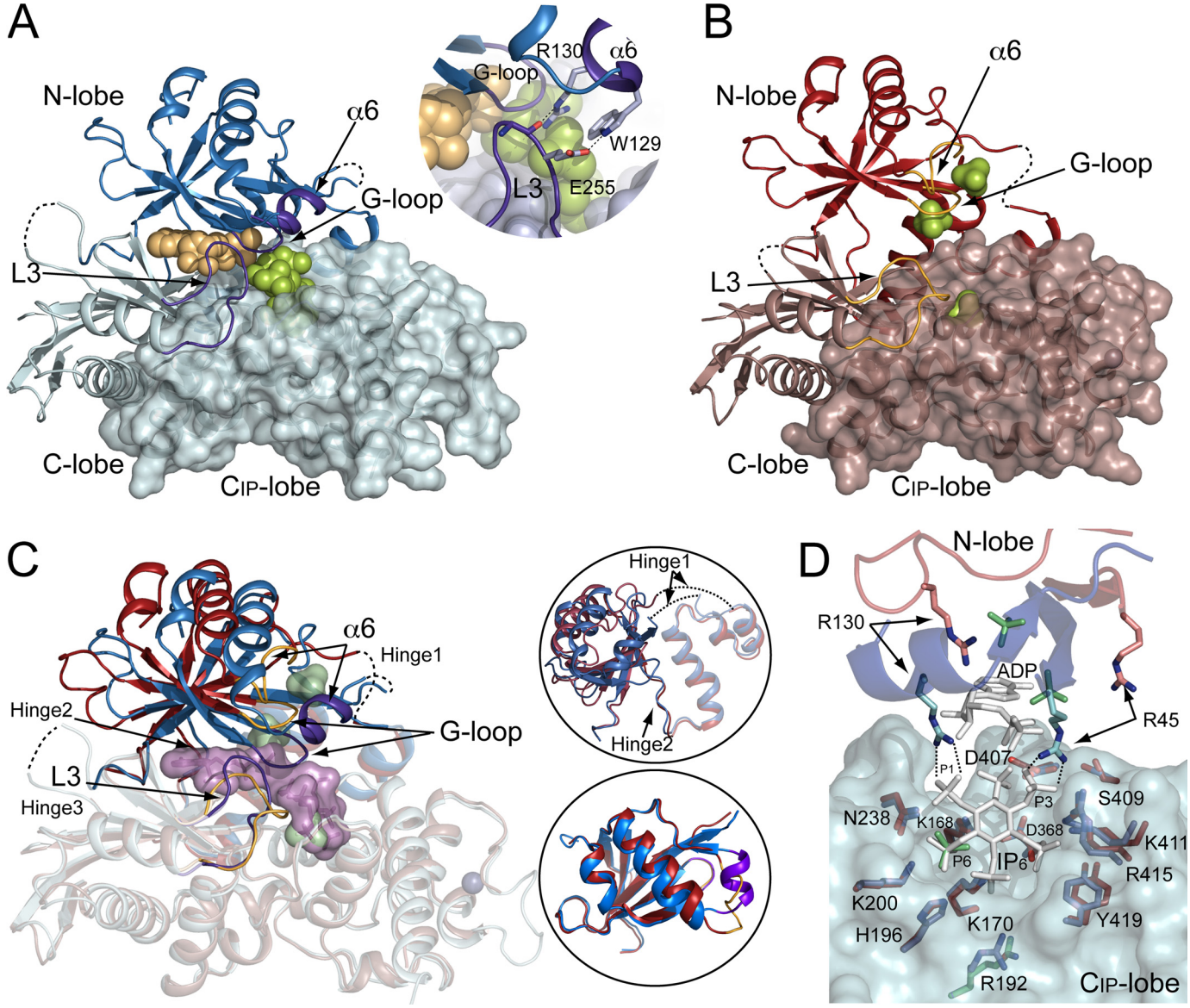

FIGURE 1. **Structure of IP$_5$ 2-K open form *versus* closed form.** *A,* IP$_5$ 2-K closed form structure, IP$_5$ 2-K complex with ADP and IP$_6$. The N-lobe and C-lobe are shown as *blue* and *light blue* schematics, respectively. The C$_{IP}$-lobe is shown as surface representation. ADP and IP$_6$ are shown as *orange* and *green spheres,* respectively. Disordered loops are shown as *dashed lines.* The key elements that close the active site (G-loop, α6, and L3) are shown in *purple-blue.* On the *top right*, a zoom of the above elements is shown, showing a detail of the interaction between α6 (N-lobe) and L3 (C-lobe). This interaction forms a clasp, joining both lobes and closing the active site. *B,* schematic representation of IP$_5$ 2-K open form as seen in the W129A mutant structure. The N-lobe and C-lobe are represented as *dark* and *light red colors*. The C$_{IP}$-lobe is highlighted with surface representation. Elements involved in covering the active site in the closed form are pointed out and are highlighted in *orange color*. Three sulfate molecules are represented as *green* surface. Disordered loops are shown as *dashed lines*. *C,* superposition of IP$_5$ 2-K open (*red colors*) and closed (*blue colors*) forms. The conformational changes upon inositide binding are well illustrated when superposing a region containing the C-lobe and segment N-I (shown as *transparent* schematics). In this superposition, a movement of a large portion of N-lobe is highlighted. Substrates in the closed form are shown as *violet transparent* surface, and sulfate ions observed in the open form are shown as *green* surface. The three hinges of the structure are also marked. The *top right panel* zooms the N-lobes of both forms, where the two regions can be appreciated as follows: a nonrotated (*transparent*) and a rotated region (*solid*), both being connected by hinges I and II. The *bottom right panel* shows a superposition of the rotated regions within the N-lobe (residues 6–42 and 103–148 from N-lobe) showing that additional local changes occur upon inositide binding, mainly at α6. *D,* inositide-binding site differences in open (*red*) and closed (*blue*) forms. The superposition made is similar to *C*. Both N-lobes are shown as schematic representation and the C-lobe as a transparent surface. The inositide ligands are shown as *stick* representation. No major variation is found in the C-lobe residues involved in inositide binding, and the N-lobe residues are farther apart in the open form, revealing that the inositide site is not fully formed in the open form. ADP and IP$_6$ in the complex are shown as *white sticks*, and the three sulfate moieties of open form are shown as *green sticks.* The G-loop is also involved in inositide binding but is not shown for clarity.

zoom), and their conformation is dependent on the clasp formation.

A detailed comparison of open and closed IP$_5$ 2-K forms reveals that the C$_{IP}$-lobe pocket remains unaltered upon inositide binding (Fig. 1*D*). Therefore, we can assume that the major inositide-binding site is preformed in the apo-form. However, this site is not fully created in the open form because the N-lobe is too far away to accomplish inositide recognition. This recognition involves interactions with the side chain of residues Arg^{45} and Arg^{130} and the main chain of the G-loop (Fig. 1*D*).

A last interesting feature is the presence of three sulfate ions in the crystal at positions similar to those occupied by Pγ (ATP)

TABLE 2

Activity of wild type and mutant IP$_5$ 2-K toward Ins(1,3,4,5,6)P$_5$

Assays were performed at 4 μM IP$_5$, 100 μM ATP. Results obtained from initial rate measurements are expressed relative to the activity of wild type enzyme assayed on the same microplate, mean ± S.D. of three experiments with 4–5 replicate measurements per experiment.

	Mean	S.D.
Wild-type	100	
R45A	58	10
W129A	121	11
W129V/R130A	21	11
R130A	16	9
ΔSer^{253}/ΔGlu^{255}	327	36

and by P1 and P6 (inositide), as found in the IP$_5$ 2-K ternary complex structure (Fig 1, *B* and *D*). These sulfate moieties, present in the crystal buffer, mimic the binding positions of the substrate in the open form of IP$_5$ 2-K.

IP$_5$ 2-K Nucleotide-bound Structure Presents a Half-closed Conformation—In our previous work, we have reported the structure of IP$_5$ 2-K ternary complexes with either substrates (IP$_5$ + AMPPNP) or products (IP$_6$ + ADP) bound at the active site (21, 24). The structure of these ternary (nucleotide + inositide) complexes revealed a common conformation with inositide-IP$_5$ 2-K binary complexes. However, the permanent presence of the inositide in our crystals precluded the assessment of specific conformational changes produced upon ATP binding. A new full crystal screening allowed us to crystallize W129A IP$_5$ 2-K with the nucleotide (ATP or ADP) (28). Although these crystals appeared in very different conditions and show different cell parameters with respect to the apo-form, they present the same space group and crystal packing. Superposition of the nucleotide-bound coordinates to those corresponding to the open and closed conformations of IP$_5$ 2-K shows that the enzyme is in an intermediate state somewhere between the apo-form (r.m.s.d. = 1.47 Å) and the closed form adopted by the ternary complex (r.m.s.d. = 1.71 Å) (Fig. 2*A*). Therefore, IP$_5$ 2-K reaches a half-closed conformation upon ATP binding that corresponds to a 10° rotation of the same portion of the N-lobe described above. We refer to this form as the "nucleotide-bound" or "half-closed" form. The ATP-binding site formed is essentially the same as that found in the ternary complexes, with only two significant differences as follows. First, in the absence of inositide there is no evidence of Mg^{2+} binding in the electron density map. This could be due to the different lobes of orientation in this form, which conforms a Mg^{2+}-binding site slightly distorted as compared with that observed in the closed form. Second, a small tilt in ATP position is observed upon inositide binding with a better fit of the nucleotide into a slightly more closed pocket in the ternary complex (Fig. 2*B*). Despite this, the nucleotide pocket formed conserves all the essential features of the nucleotide recognition by the protein kinase superfamily, revealing that this conformation is physiologically relevant. In contrast, the C_{IP}-lobe remains unaltered upon nucleotide binding, and the N-lobe, although closer, is still too far away to complete the inositide-binding site; consequently, the clasp observed in the closed-form is not formed.

In the half-closed form that we obtained with nucleotide, sulfate ions were found bound in similar positions to that occupied in the closed form by inositide phosphates P1, P6, and P5 (Fig. 2*A*). These sulfates putatively mimic the binding of inositide in this half-closed form. Finally, unlike what was observed in the open and closed conformations, hinge 1 and hinge 3 are ordered in this form.

Snapshots of the Conformational Changes—The crystal structures of the two IP$_5$ 2-K states here reported, together with our previous work (24), provide more detail of the enzymatic mechanism. Our experimental results reveal essential structural motions associated with nucleotide and inositide binding that not only involve a large movement of two protein portions as rigid bodies but also local changes on the clasp region (Fig. 3). As predicted before, the clasp is fully formed only in the closed state by interaction of L3 (from the C-lobe) and α6 (from the N-lobe), through Trp^{129}–Glu^{255} and Arg^{130}–Gly^{254} links (Fig. 3*A*, *right*). The formation of this clasp requires the rupture of the Glu^{255}–Lys^{200} ion pair that links L3 to the C_{IP} lobe, in both the open and nucleotide-bound conformations (Fig. 3*A*, *left* and *middle panels*). This breakage releases L3 to act as the "lid" that closes the pocket upon inositide binding. The conformation of both α6 and L3 changes significantly among the different structural states of IP$_5$ 2-K (Fig. 3*A*). In fact, the segment α6 is not structured in the open conformation; the helix is fully formed only in the closed state. In addition, L3 is rearranged in the closed state, taking an extended conformation formed by a new pattern of interactions with IP$_5$ 2-K residues of loop Thr^{235}–Asn^{239} (L2), where the conserved ^{237}QNN motif is located (Fig. 3*B*). Thus, the interaction Asn^{238}–Arg^{241} observed in the open and half-closed conformation is broken leaving L2 able to interact with L3 through Gln^{237}–Thr^{257} and Asn^{238}–Ser^{256} links. Consequently, most of the structural changes observed in IP$_5$ 2-K are due to inositide binding, but it is worth mentioning that in the nucleotide-bound form the clasp seems partially created through interaction of Arg^{130}(α6) and Gly^{252}(L3).

Clasp Role—As shown in Table 2, we have measured the activity of several IP$_5$ 2-K mutants of clasp-contributing residues to assess their contribution to the enzymatic mechanism. Assays were performed by a coupled enzyme assay allowing steady-state measurements. In particular, we have analyzed the effect of single and double substitutions in α6 key residues (W129A, R130A, and W129V/R130A) and deletions in L3 (ΔSer^{253}/ΔGlu^{255}). First, the activity of the W129A mutant is uncompromised leading to the conclusion that Trp^{129} participation in clasp formation is not critical for enzyme activity. It is worth noting that the bond formed by Trp^{129} in the clasp is not the unique determinant for the clasp formation. Second, mutation of Arg^{130} results in more than 6-fold decreased activity toward Ins(1,3,4,5,6)P$_5$ and toward other substrates (see below), and the double mutation W129V/R130A results also in a 5-fold reduced activity, a fact that could be ascribed mainly to the Arg^{130} mutation. Arg^{130} is involved in both clasp formation and inositide binding through P1 (Figs. 1*D* and 5); therefore, its contribution may be more critical for enzyme function. Finally, shortening of L3 by two residues (ΔSer^{253}/ΔGlu^{255}) results in an IP$_5$ 2-K mutant 3-fold more active that the native form. Modeling this shorter loop in the IP$_5$ 2-K structure suggests that deletion of these two residues precludes clasp formation. We suggest that the increased activity may be attributed to an improved kinetics of the enzyme, perhaps through removal of

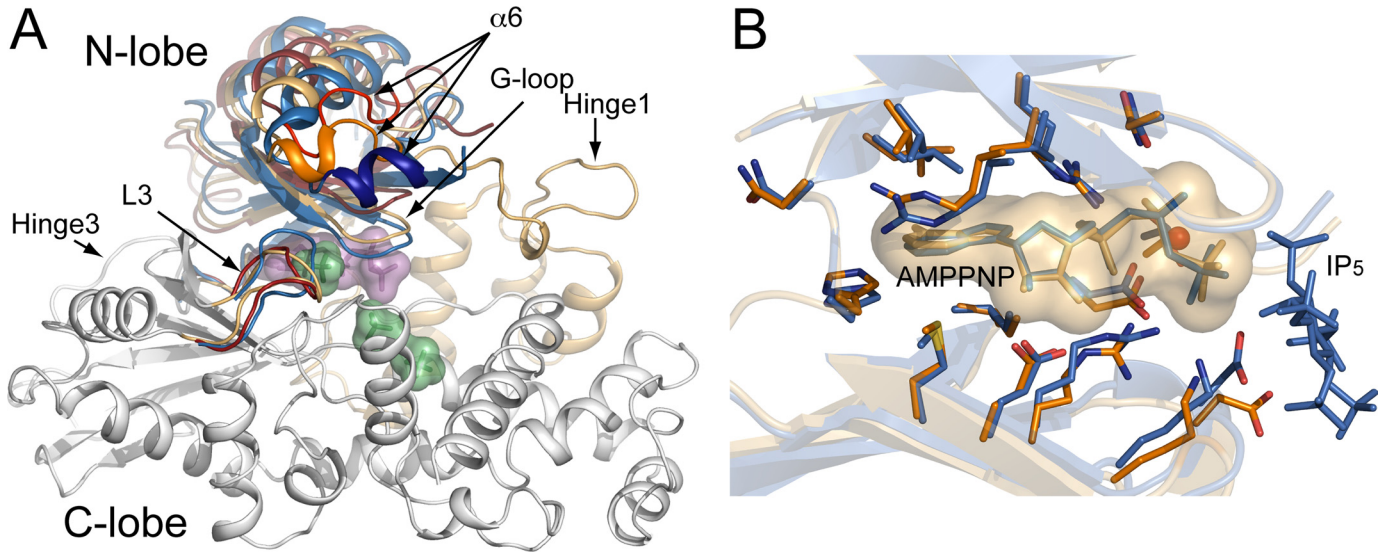

FIGURE 2. **Conformational changes upon nucleotide binding.** *A,* comparison of the three IP_5 2-K obtained conformations (open, half-closed, and closed forms). The superposition has been made on the C-lobes and segment N-I as before. The IP_5 2-K nucleotide-bound form is shown as *orange* (N-lobe) and *white* (C-lobe) schematics. The nucleotide and the sulfate moieties found in this form are shown as *transparent violet* surface and *green* surface, respectively. As the C-lobes superpose very well in the three cases, only the rotated N-lobe region and L3 have been shown for the open (*red*) and closed (*blue*) forms. This picture highlights the sequential structural changes upon nucleotide and inositide binding, as well as the clasp elements variation. *B,* comparison between the nucleotide-binding site as shown in the half-closed (*orange*) and closed (*blue*) forms. The superposition has been made by matching the ATP molecules. The ATP-binding site is very similar in both structures, although it is more constrained in the closed form. Magnesium found in the closed form is shown as *red sphere*.

the lid, that would decrease the energetic barrier of the process, for instance through a more favorable release of products.

As mentioned above, we have shown that W129A-IP_5 2-K retains as much activity as the native enzyme (Table 2). We have performed kinetic measurements for native and W129A IP_5 2-K (Fig. 4 and Table 3). Our results show that, although there are no dramatic changes, the native IP_5 2-K presents ~3-fold greater affinity for the inositide substrate ($K_{m,\,app}$ 3.7 ± 1.0 μM) than the mutated enzyme (13.7 ± 3.0 μM). However, $V_{max,\,app}$ of W129A mutant (0.95 ± 0.16 μmol min^{-1} mg^{-1}) is 2-fold higher than that of the native enzyme (0.54 ± 0.07 μmol min^{-1} mg^{-1}), telling us that the mutant is more efficient. The removal of the Trp^{129} side chain probably affects the inositide binding pocket formation, as it is next to Arg^{130}. In turn, Trp^{129} removal likely weakens clasp formation producing a more efficient enzyme, which correlates with our previous suggestion that lid removal could be favoring the product release.

Role of the N-lobe in Inositide Binding and Specificity—Inositol 1,3,4,5,6-pentakisphosphate is bound to the N-lobe through phosphates P1 (Arg^{130}) and P3 (Arg^{45} and G-loop main chain) (Fig. 1*D*). To assess the importance of P1 and P3 to inositide binding and ensuing conformational change, we made several attempts to crystallize IP_5 2-K in presence of the enantiomers Ins(3,4,5,6)P_4 and Ins(1,4,5,6)P_4, which are expected to bind in the same orientation as Ins(1,3,4,5,6)P_5. The presence of a plane of symmetry along the C2-C5 axis of Ins(1,3,4,5,6)P_5 allows, in comparison with the two IP_4s, an assessment of the contribution of residues coordinating the enantiotopic 1- and 3-phosphates.

We obtained crystals of IP_5 2-K in ternary complex with Ins(3,4,5,6)P_4 and AMPPNP. These crystals turned out to be similar to the previously solved ternary complexes and binary complexes of IP_5 2-K and inositide (r.m.s.d.. 0.425 Å) (24) and confirm that Ins(3,4,5,6)P_4 binds in the same orientation as Ins(1,3,4,5,6)P_5 (Fig. 5). The most interesting feature of the new ternary complex is that Arg^{130} is perfectly oriented to potentially bind the absent P1, and it maintains interaction with L3 forming the clasp as in IP_5-bound structures. This result suggests that Arg^{130} participation in P1 binding and clasp formation represents two separate facets of IP_5 2-K function. As mentioned before, the R130A mutant presents reduced but significant IP_5 2-K activity, suggesting that although Arg^{130} is an important residue, it is not essential for catalysis. In parallel, as we were unsuccessful in attempts to grow crystals in the presence of inositide lacking P3 (Ins(1,4,5,6)P_4), we have generated an R45A IP_5 2-K mutant to remove one of P3 binding residues (Figs. 1*D* and 5). The fact that R45A retains appreciable activity against Ins(1,3,4,5,6)P_5 suggests that Arg^{45}, although not essential, makes some contribution to inositide binding. As P3 of both Ins(1,3,4,5,6)P_5 and Ins(3,4,5,6)P_4 are bound to the protein G-loop, it seems likely that the G-loop plays a main role in inositide binding and in subsequent conformational changes.

Because there remains conjecture concerning the relative contribution of different pathways to IP_6 synthesis in plants (19), and because Ins(1,4,5,6)P_4 and Ins(3,4,5,6)P_4 have been reported to be substrates *in vitro* of plant enzymes (6, 18), we have compared the activity of IP_5 2-K toward Ins(1,4,5,6)P_4 and Ins(3,4,5,6)P_4 for native protein and for a range of mutants in N-lobe residues. Our assays were performed at a fixed concentration of inositol phosphate (5 μM) and ATP (100 μM) (Table 4). Ins(3,4,5,6)P_4 and Ins(1,4,5,6)P_4 are equally active substrates for IP_5 2-K. The ratio of activity against Ins(1,4,5,6)P_4/Ins(3,4,5,6)P_4 is increased significantly by the R45A mutation and reduced slightly by W129A mutation. However, and remarkably, substitution involving Arg^{130} (R130A) increase

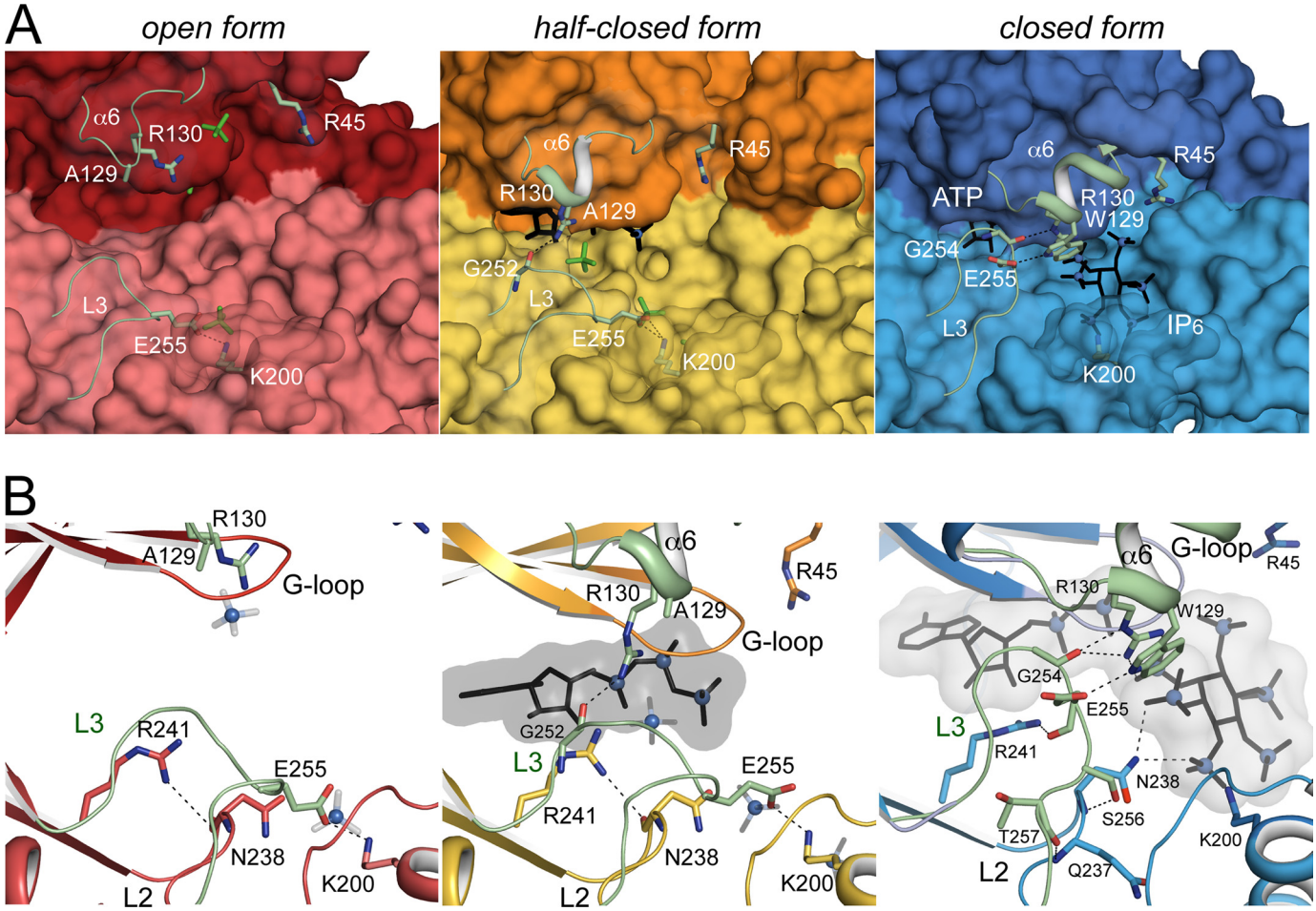

FIGURE 3. **Snapshots of the different IP$_5$ 2-K conformations.** *A*, sequential view of IP$_5$ 2-K active site structure in open (*red*), half-closed (*orange*), and closed (*blue*) forms. The N- and C-lobes are distinguished by different color shades. The key protein elements that cover the active site and that change conformations between the different forms (G-loop, L3, α6) are highlighted in *green*. Interactions for clasp formation in the closed form as well as the singular intramolecular ion pair (Asp^{255}–Lys^{200}) in open and half-closed forms are highlighted. Sulfate moieties are shown as *green sticks*. *B*, IP$_5$ 2-K active site along its different forms represented as *sticks* and following the code colors of *A*. Specific interactions formed and broken upon nucleotide and inositide binding are shown. Sulfates and substrates are shown as *black sticks*, highlighting phosphates and sulfate atoms as *blue spheres*.

markedly the discrimination of the enzyme in favor of Ins(3,4,5,6)P$_4$. These results highlight the importance of Arg^{130} in P1 binding. We are not aware of other structure-based studies of discrimination between enantiomeric substrates in inositol phosphate kinases.

Intrinsic Fluorescence Decreases upon Substrate Binding—The new structures that we have obtained provide description of conformational changes consequent upon ligand binding. We have undertaken ligand binding analysis of native and W129A mutants by fluorescence. For this purpose, we titrated Ins(1,3,4,5,6)P$_5$ substrate and recorded changes in intrinsic tryptophan fluorescence, exciting at 295 nm to limit fluorescence to tryptophan residues. We performed similar experiments titrating the nucleotide analog AMPPNP. Before performing substrate/analog titrations, we undertook Stern-Volmer analysis of quenching of tryptophan fluorescence with iodide as the quencher. The linearity of the unmodified Stern-Volmer plot and the *y* axis intercept of 1.03 for native and 1.02 for W129A (data not shown) indicate that the tryptophan residues of native and W129A protein are all accessible to the quenching agent. We also assessed the temperature dependence of fluorescence quenching by iodide. The increased gradient and linearity of the plot at higher temperature indicate that the quenching process is collisional. These data are compatible with all tryptophans solvent-exposed in native and W129A protein. IP$_5$ 2-K has a total of four tryptophan residues among which two of them are on protein surface but partially buried in an hydrophobic pocket (Trp^{13} and Trp^{69}), although the other two are totally exposed (Trp^{129} and Trp^{381}). More precisely, Trp^{129} would change its conformation from a partially exposed (closed form) to a completely exposed (open form, mutated by Ala) upon binding.

Incremental addition of Ins(1,3,4,5,6)P$_5$ yielded a saturating decrease in fluorescence for both native and W129A IP$_5$ 2-K (Fig. 6, *A* and *B*). Although it is clear that the decrease in fluorescence for the W129A mutant arises from residues other than tryptophan Trp^{129}, that for native protein additionally includes Trp^{129}. Fluorescence decreases in both cases are moderate. Assuming that Trp^{281}, permanently solvent-exposed, is not a main contributor, the moderate changes are in concordance with slight distortions produced in Trp^{13} and Trp^{69} pockets upon inositide binding observed in the crystals. Plots of fractional change in fluorescence *versus* ligand such as that shown for native protein (Fig. 6*C*) yielded K_d values for Ins(1,3,4,5,6)P$_5$ of 0.35 ± 0.12 μM for native protein and 0.42 ± 0.03 μM for W129A IP$_5$ 2-K. These data show that binding of

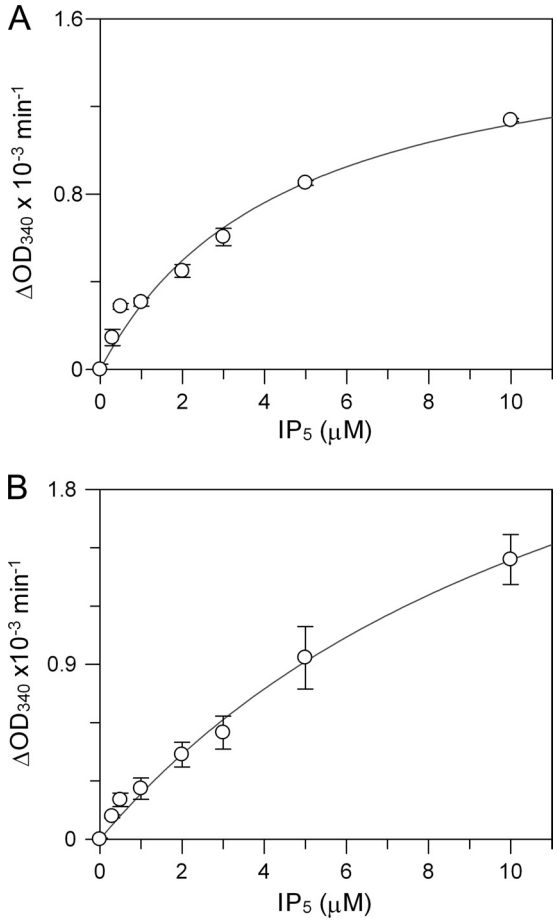

FIGURE 4. **Kinetic analysis of IP$_5$ 2-K.** Enzyme activity was assayed by a coupled enzyme assay. Titration of Ins(1,3,4,5,6)P$_5$ yielded saturating increase in enzyme activity of native (*A*) and W129A IP$_5$ 2-K (*B*). Progress of reaction curves were fitted by nonlinear regression to the Michaelis-Menten equation. The data in the text provide the mean ± S.D. of kinetic parameters determined in three independent experiments with 4 to 5 replicate samples.

TABLE 3

Kinetic parameters of wild type and W129A IP$_5$ 2-K

Kinetic parameters were determined by nonlinear least squares fitting to the Michaelis-Menten equation of plots of reaction velocity *versus* Ins(1,3,4,5,6)P$_5$ concentration, mean ± S.D. of three experiments with 4 to 5 replicates per experiment.

	$V_{max\ app}$	$K_{m,\ app}$
	μmol/min/mg	*μM*
Wild type	0.54 (0.07)	3.7 (1.0)
W129A	0.95 (0.16)	13.7 (3.0)

Ins(1,3,4,5,6)P$_5$ causes conformational change in IP$_5$ 2-K (either wild type or mutant), a result consistent with differences in conformation found between ligand-free and IP$_5$ 2-K inositide-bound structures. Remarkably, the affinity for inositide is similar in both proteins.

Titrations of AMPPNP also gave a saturating decrease in fluorescence, again for both native and W129A IP$_5$ 2-K (Fig. 6, *D* and *E*). Plots of fractional change in fluorescence *versus* ligand such as that shown for native protein (Fig. 6*F*) yielded K_d 37 ± 9 μM and 55 ± 2 μM, respectively, for native and W129A protein. These structural changes reported by fluorescence upon AMPPNP binding are in agreement with the crystallographic differences in conformation between W129A IP$_5$ 2-K ligand-free and in complex with the nucleotide. The affinities for the

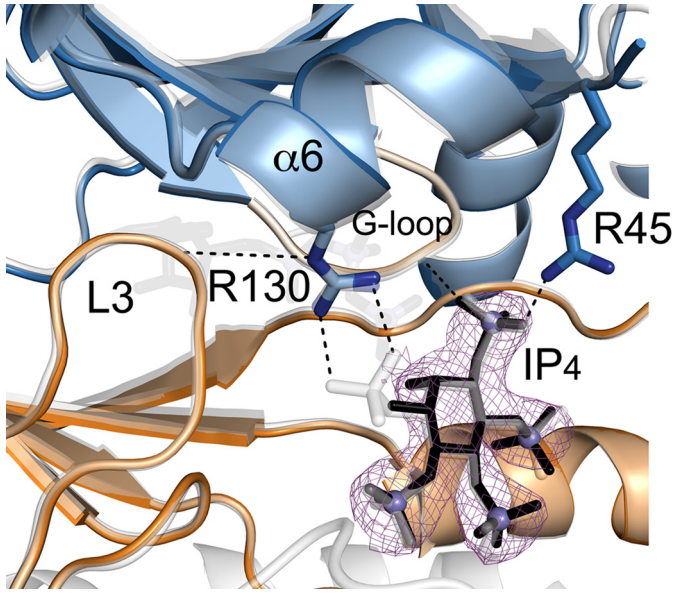

FIGURE 5. **IP$_5$ 2-K binary complex with AMPPNP and Ins(3,4,5,6)P$_4$.** The N-lobe is shown in *blue*, the C-lobe in *orange*, and IP$_4$ as *black sticks* with phosphates highlighted as *slate spheres* (AMPPNP is shown as *transparent sticks*). The superposed IP$_5$ 2-K·AMPPNP·IP$_5$ complex (Protein Data Bank code 2xan) is shown as *transparent white* schematics and *sticks*. The inositide ligands from the N-lobe are shown as *blue sticks*. All protein interactions with inositide are retained with the exception of Arg^{130}-P1 formed with IP$_5$. However the position of Arg^{130} is the same, and the interaction with L3 is conserved in this complex.

TABLE 4

Relative activities of IP$_5$ 2-K mutants for enantiomeric Ins(1,4,5,6)P$_4$ and Ins(3,4,5,6)P$_4$ substrates

Activities of mutants are expressed relative to the activity of wild-type enzyme assayed on the same microplate. Results obtained from initial rate measurements are also expressed as a ratio of enzyme activities against the enantiomeric substrates Ins(1,4,5,6)P$_4$/Ins(3,4,5,6)P$_4$. Assays were performed at 5 μM IP$_4$, 100 μM ATP. The experiment has been repeated three times with similar results. A similar experiment with a different batch of substrate yielded Ins(1,4,5,6)P$_4$/Ins(3,4,5,6)P$_4$ ratios for WT, 0.64 ± 0.04; W129A, 0.58 ± 0.03, and W129V/R130A, 0.10 ± 0.05.

	Ins(1,4,5,6)P$_4$		Ins(3,4,5,6)P$_4$		Ratio	
	% of WT	S.D.	% of WT	S.D.	Mean	S.D.
Wild type	100		100		0.99	0.15
R45A	179	23	135	8	1.31	0.17
W129A	75	7	97	15	0.77	0.12
R130A	17	7	59	5	0.28	0.07

nucleotide showed by the wild type and W129A IP$_5$ 2-K are quite similar, although slightly decreased for the W129A protein. Because the clasp would not be properly formed in this mutant, probably a less stable nucleotide complex is formed.

DISCUSSION

We have obtained different snapshots of IP$_5$ 2-K functional states (Figs. 2*A* and 3) by x-ray crystallography. Each different state is unequivocally correlated with binding of nucleotide or inositide at the active site. Thus, the protein shows an open conformation in the absence of substrates, a half-closed conformation when bound to nucleotide, and as reported previously (24), a closed conformation in the inositide-bound state. In agreement with the crystal structures presented here, IP$_5$ 2-K intrinsic fluorescence decreases upon nucleotide and inositide binding (Fig. 6). We have predicted previously such conformational changes (24). Very recently, some experimental evidence of these changes has been reported by partial proteolysis exper-

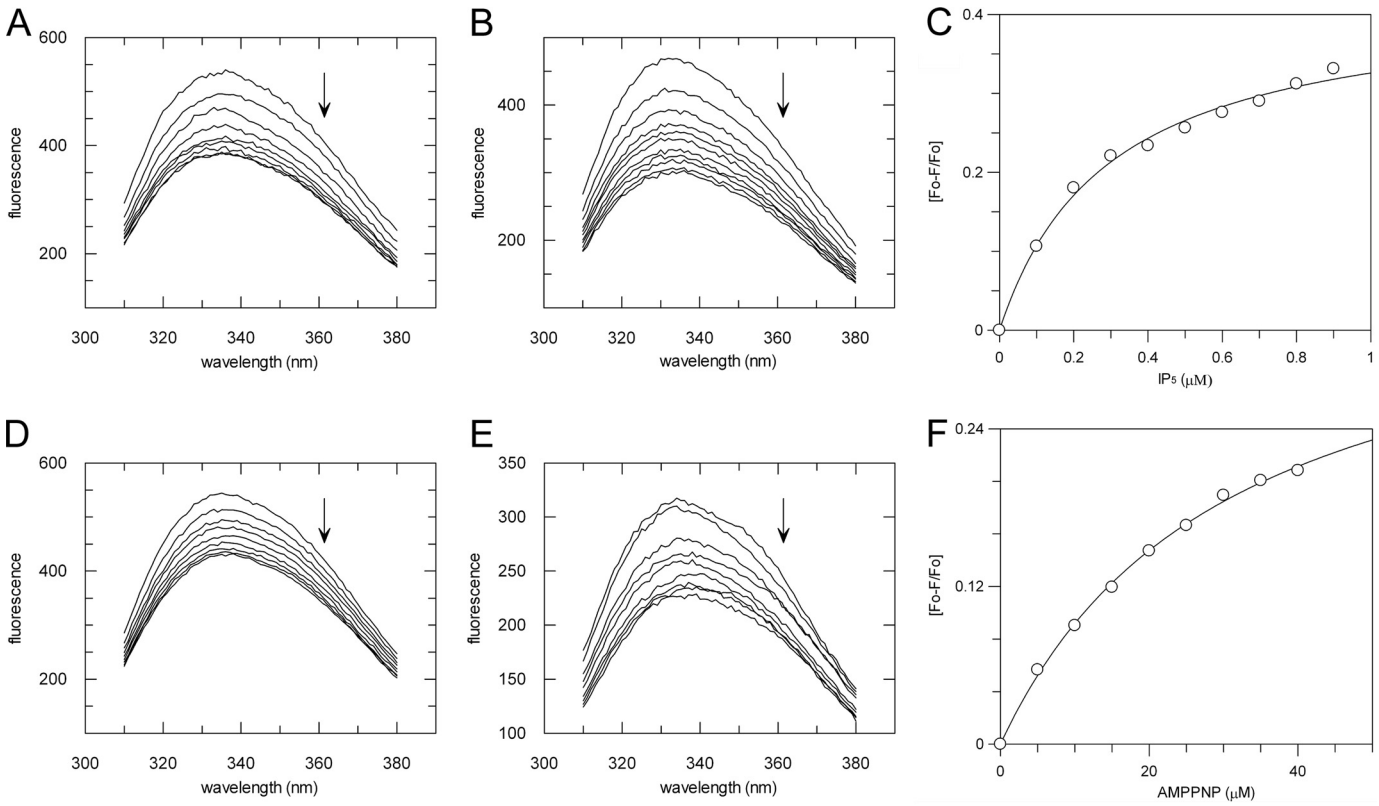

FIGURE 6. **Ligand binding to IP$_5$ 2-K.** Titration of Ins(1,3,4,5,6)P$_5$ (*A* and *B*) or AMPPNP (*D* and *E*) yielded saturating decreases in intrinsic fluorescence of native (*A* and *D*) and W129A IP$_5$ 2-K (*B* and *E*). *Arrows* indicate the direction of change of fluorescence on incremental additions of ligand. Plots of fractional change in fluorescence are shown for native protein *versus* Ins(1,3,4,5,6)P$_5$ (*C*) and *versus* AMPPNP (*F*).

iments that show stabilization of some regions of IP$_5$ 2-K upon inositide and nucleotide binding (40). This work shows that high resolution analysis of the conformational events has been possible by a single mutation (W129A) allowing description of a complete picture of the different conformational states experienced by IP$_5$ 2-K throughout the substrate binding stages of catalysis. The assumption that the W129A mutant is a mimic of WT IP$_5$ 2-K is based on the experimental evidence presented here. In addition, the W129A mutant presents similar protection from proteolysis in the presence of nucleotide and inositide as wild type IP$_5$ 2-K, as well as a similar band shift on native gels in presence of IP$_6$ (data not shown).

Inositide Alone Can Promote Closed Conformation and Clasp Formation—An intriguing aspect from our studies is that inositide is sufficient and necessary to trigger the closed conformation and complete the clasp formation, and it can do so independently of ATP binding. We were able to crystallize IP$_5$ 2-K with AMPPNP/Ins(3,4,5,6)P$_4$ in the closed form; however, trials with AMPPNP/Ins(1,4,5,6)P$_4$ were unsuccessful. One potential explanation of these observations is that the inositide P3 coordination to Arg^{45} and/or the G-loop is essential to favor the closed form upon inositide binding (Fig. 5). In fact, because Arg^{45} mutation does not significantly compromise enzyme activity, we suggest that the G-loop may be the principal N-lobe element for inositide binding and subsequent conformational changes. In addition, the clasp is fully formed only in the closed conformation. Mutation of clasp elements that would preclude its formation yield active enzymes, suggesting that the clasp formation is not essential for protein activity (Table 2). On the contrary, the clasp might be relevant for modulating protein kinetics as suggested by enzymatic and kinetic measurements. In conclusion, both events, domain closure and clasp formation, are coupled to inositide binding, and the G-loop could be playing a direct role in the conformational changes. A main role for a G-loop has been largely studied in protein kinases, where it has been suggested that it is a regulatory flap above the ATP-binding site showing great flexibility (41, 42).

In this closed form, the inositide blocks the nucleotide entrance/exit to/from the active site. This suggests that the nucleotide might bind first, producing a half-closed conformation, and the inositide later completed the domain closure. Then the product release should proceed in an inverse order, because the nucleotide is completely occluded in the inositide-bound form. The exit of ADP could be the limiting step for IP$_5$ 2-K activity, as it has been reported for PKs (43), because the motion to open the domains and/or to undo the clasp is necessary for nucleotide release. These suggestions are supported by the fact that clasp-affected mutants as W129A or ΔS253/ΔE255 produce more efficient or active proteins. Nevertheless, more work has to be done to confirm these entire hypotheses about substrate binding order. We consider that the capacity of inositide alone to trigger the closed conformation could reflect its role as an enzyme inhibitor and therefore in regulation of enzymatic activity. Several examples of similar proteins being inhibited by its substrate/product can be found in the literature (44–47).

Modulation of Enantiomeric IP$_4$ Preference of Plant IP$_5$ 2-Ks—The relative contribution of different pathways to IP$_6$ synthesis in plants is the focus of much attention (18, 19). We

have compared the activity of IP$_5$ 2-K toward Ins(1,4,5,6)P$_4$ and Ins(3,4,5,6)P$_4$ for native protein and for a range of mutants, because both enantiomers represent intermediates in disparate pathways reported to proceed from inositol 1,4,5-trisphosphate and inositol, respectively (19). Ins(1,4,5,6)P$_4$ is a product of plant multikinase action against inositol 1,4,5-trisphosphate, certainly *in vitro* (48, 49). *At*IPK2β, a multikinase, and *At*IPK1 (IP$_5$ 2-K) contribute to IP$_6$ synthesis in *Arabidopsis* (18). Ins(3,4,5,6)P$_4$ was identified in early studies of IP$_6$ synthesis in duckweed (50). This isomer is a substrate of plant ATP-grasp fold inositol tris/tetrakisphosphate kinases (20, 51–53), and enzymes of this class contribute to IP$_6$ synthesis in maize (20). We have shown using a coupled assay that Ins(3,4,5,6)P$_4$ and Ins(1,4,5,6)P$_4$ are equally effective *in vitro* substrates for IP$_5$ 2-K, and we have now determined the role of Arg^{130} and Arg^{45} in the specification of substrate preference between enantiomers. We note that although Arg^{130} is fully conserved across kingdoms, Arg^{45} is not, and within plants the equivalent residue is variable (6). Moreover, despite the elucidation of structures of a variety of inositol phosphate kinases belonging to the ATP-grasp fold and inositol polyphosphate kinase families, this is the first study in which discrimination between enantiomeric substrates has been investigated. Our choice of substrates, although dictated by consideration of what is known of inositol phosphate metabolism in plants, is of obvious relevance to animal inositol phosphate metabolism centered on the same enantiomers. In addition, manipulation or inverting the enantiomeric substrate preference and therefore enantiomeric product production is of great interest from a chemical and a biotechnological point of view.

Singular Enzyme among the Inositide Kinase Family—The structural features for all inositide kinase families have been extensively studied to determine the structural determinants of substrate specificity. Structures are available for different inositol phosphate kinases in the presence/absence of substrates and products, providing data about structural changes produced upon binding of nucleotide and/or inositide. With respect to the IPK family, to which IP$_5$ 2-K belongs, none of the structures solved up to now (IP$_3$ 3-K (21, 22) and IPmK (23)) show significant structural changes upon nucleotide binding. However, data upon inositide binding is only known for IP$_3$ 3-K, for which a slight conformational change is described. This change consists of an inositide site rearrangement achieved by a protein intramolecular bridge breakage between the C-lobe and IP-lobe (Arg^{419}–Asp^{374}) leaving Arg^{419} free to interact with inositide. As seen in IP$_5$ 2-K, a bond is also broken upon inositide binding (Lys^{200}–Asp^{255}) to leave Lys^{200} able to bind inositide. Nevertheless, the bridges in the two proteins are not structurally related, and IP$_3$ 3-K does not present structurally equivalent elements of L3 or α6. In any case, the conformational change produced in IP$_3$ 3-K is local, and it does not involve large movements between domains as in IP$_5$ 2-K. A member from the other family of inositol phosphate kinases, those from ATP-grasp fold, also shows structural differences upon inositide binding. In the recent published structure for the pyrophosphate inositol-synthesizing enzyme PPIP5K (26), the side chain of three large basic residues changes markedly upon inositide binding, revealing a major reorganization in the inositide-binding site configuration without involving backbone changes. In conclusion, this is the first time that such a conformational change involving domain movements upon inositide as well as nucleotide binding is shown for a member of the inositol phosphate kinase family. However, we must not ignore the fact that it has not yet been possible to crystallize every inositol kinase and in all their different states. Thus, none of the IP$_6$ K isoforms structures are available at the moment and neither are the IPmKs in the presence of inositide nor PPIP5K in the absence of nucleotide. Consequently, the possibility of undetermined conformational changes for these families of enzymes cannot be precluded.

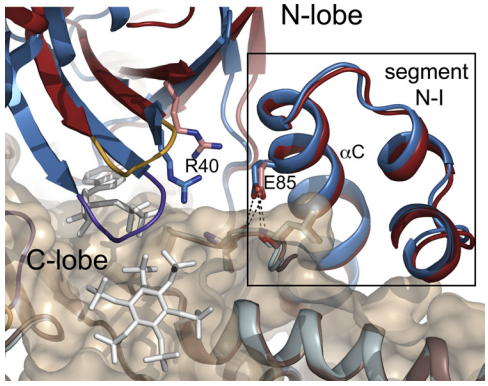

FIGURE 7. **IP$_5$ 2-K αC and C-lobe are coupled during domain motions.** The IP$_5$ 2-K N-lobes are shown as *red* (open form) and *blue* (closed form) schematics, respectively. The C-lobe is shown as surface representation. Element N-I αC is *squared*. Glu^{85} does not form a bridge with Arg^{40}, unlike the situation in PKs in active conformation. Glu^{85} maintains interaction with the C-lobe through the motion. The residues involved are shown as *sticks*.

Comparison with Protein Kinases—A similar domain movement has been reported for protein kinases (42, 54). In the most studied PK (PKA), the nucleotide binding generates a closure between both N- and C-lobes (43). In our previous work (24), we reported that the distinctive bridge linking αC and the N-lobe β3 in PKAs structures representing the active conformation (Lys^{72}–Glu^{91}) is not formed in IP$_5$ 2-K (Arg^{40}–Glu^{85} equivalent residues); therefore, we suggested that the bridge is not a hallmark for active conformation in IP$_5$ 2-Ks (Fig. 7). On the contrary, interaction between αC and the C-lobe is retained in both PKAs and IP$_5$ 2-Ks. Thus, in concordance with our previous results, the IP$_5$ 2-K open and half-closed conformations also lack this bridge, and in the domain motion reported here, the N-lobe region containing αC (N-I) is coupled with the C-lobe (Fig. 7), whereas in PKA the motion from open to close conformations keeps αC in contact with both lobes (43).

Conclusions—From our previous inositide-bound IP$_5$ 2-K structure (closed form) and using a rational approach, we have designed several IP$_5$ 2-K mutations prone to yield an open protein conformation. From a specific protein mutant, W129A, we have conducted crystallization of IP$_5$ 2-K in an open, free of substrates, and a half-closed nucleotide-bound conformation. Combining this information with the known closed inositide-bound form, we have provided a schematic view of the conformations adopted by IP$_5$ 2-K in the course of IP$_6$ synthesis. This is the first time that such a conformational change is reported for an inositide kinase. Moreover, these changes explain all the experimental observations, including fluorescence measurements, that pointed to a nucleo-

tide- and inositide-induced conformational changes in IP_5 2-K. The different protein forms captured can be considered as a "biological mimic state," proving mutagenesis to be a successful tool in Protein Crystallography.

A general problem facing the protein kinase field is the design of selective inhibitors, because all protein kinases bind ATP in a very similar manner. In the case of inositol phosphate kinases, we can use the inositide-binding site for design of specific inhibitors; however, a number of crucial inositide kinases could be affected by similar molecules. To overcome this selectivity problem and avoid off-target effects, an understanding of the structural basis of substrate specificity and preference is essential. Furthermore, a common approach is to exploit protein conformational changes to design specific inhibitors. In this context, docking studies, which start from an ensemble of different states, have been proven to be successful. The main goals of this work were to provide new substrate recognition features, as elements involved in enantiotopic phosphate discrimination and structures of different protein conformational states. These are valuable tools in the search for specific and selective protein inhibitors with potential applications as biological tools for *in vivo* studies. The implications of IP_5 2-K in crucial cellular and developmental events have been already proven; however, elaboration of protein inhibitors could help in the determination of further roles for IP_5 2-K in mammals.

Acknowledgments—We thank María Álvarez-Cao, Juana María González-Rubio, and Kendall Baker for technical assistance and the European Synchrotron Radiation Facility (Grenoble, France) for providing beam time and assistance during data collection. We thank Stephen Mills (University of Bath, UK) for the gift of Ins(1,4,5,6)P_4 and Ins(3,4,5,6)P_4 used in some of the enzyme assays described.

REFERENCES

1. Streb, H., Irvine, R. F., Berridge, M. J., and Schulz, I. (1983) Release of Ca^{2+} from a nonmitochondrial intracellular store in pancreatic acinar cells by inositol 1,4,5-trisphosphate. *Nature* **306,** 67–69
2. Irvine, R. F., and Schell, M. J. (2001) Back in the water. The return of the inositol phosphates. *Nat. Rev. Mol. Cell Biol.* **2,** 327–338
3. Ives, E. B., Nichols, J., Wente, S. R., and York, J. D. (2000) Biochemical and functional characterization of inositol 1,3,4,5,6-pentakisphosphate 2-kinases. *J. Biol. Chem.* **275,** 36575–36583
4. Phillippy, B. Q., Ullah, A. H., and Ehrlich, K. C. (1994) Purification and some properties of inositol 1,3,4,5,6-pentakisphosphate 2-kinase from immature soybean seeds. *J. Biol. Chem.* **269,** 28393–28399
5. Stephens, L. R., Hawkins, P. T., Stanley, A. F., Moore, T., Poyner, D. R., Morris, P. J., Hanley, M. R., Kay, R. R., and Irvine, R. F. (1991) Myo-inositol pentakisphosphates. Structure, biological occurrence, and phosphorylation to myo-inositol hexakisphosphate. *Biochem. J.* **275,** 485–499
6. Sun, Y., Thompson, M., Lin, G., Butler, H., Gao, Z., Thornburgh, S., Yau, K., Smith, D. A., and Shukla, V. K. (2007) Inositol 1,3,4,5,6-pentakisphosphate 2-kinase from maize. Molecular and biochemical characterization. *Plant Physiol.* **144,** 1278–1291
7. Sweetman, D., Johnson, S., Caddick, S. E., Hanke, D. E., and Brearley, C. A. (2006) Characterization of an *Arabidopsis* inositol 1,3,4,5,6-pentakisphosphate 2-kinase (*At*IPK1). *Biochem. J.* **394,** 95–103
8. Verbsky, J. W., Wilson, M. P., Kisseleva, M. V., Majerus, P. W., and Wente, S. R. (2002) The synthesis of inositol hexakisphosphate. Characterization of human inositol 1,3,4,5,6-pentakisphosphate 2-kinase. *J. Biol. Chem.* **277,** 31857–31862
9. Verbsky, J., Lavine, K., and Majerus, P. W. (2005) Disruption of the mouse inositol 1,3,4,5,6-pentakisphosphate 2-kinase gene, associated lethality, and tissue distribution of 2-kinase expression. *Proc. Natl. Acad. Sci. U.S.A.* **102,** 8448–8453
10. Alcázar-Román, A. R., Bolger, T. A., and Wente, S. R. (2010) Control of mRNA export and translation termination by inositol hexakisphosphate requires specific interaction with Gle1. *J. Biol. Chem.* **285,** 16683–16692
11. Shen, X., Xiao, H., Ranallo, R., Wu, W. H., and Wu, C. (2003) Modulation of ATP-dependent chromatin-remodeling complexes by inositol polyphosphates. *Science* **299,** 112–114
12. Sarmah, B., Latimer, A. J., Appel, B., and Wente, S. R. (2005) Inositol polyphosphates regulate zebrafish left-right asymmetry. *Dev. Cell* **9,** 133–145
13. Agarwal, R., Mumtaz, H., and Ali, N. (2009) Role of inositol polyphosphates in programmed cell death. *Mol. Cell. Biochem.* **328,** 155–165
14. Bennett, M., Onnebo, S. M., Azevedo, C., and Saiardi, A. (2006) Inositol pyrophosphates. Metabolism and signaling. *Cell. Mol. Life Sci.* **63,** 552–564
15. Murphy, A. M., Otto, B., Brearley, C. A., Carr, J. P., and Hanke, D. E. (2008) A role for inositol hexakisphosphate in the maintenance of basal resistance to plant pathogens. *Plant J.* **56,** 638–652
16. Raboy, V. (2001) Seeds for a better future. "Low phytate" grains help to overcome malnutrition and reduce pollution. *Trends Plant Sci.* **6,** 458–462
17. Raboy, V. (2003) myo-Inositol-1,2,3,4,5,6-hexakisphosphate. *Phytochemistry* **64,** 1033–1043
18. Stevenson-Paulik, J., Bastidas, R. J., Chiou, S. T., Frye, R. A., and York, J. D. (2005) Generation of phytate-free seeds in *Arabidopsis* through disruption of inositol polyphosphate kinases. *Proc. Natl. Acad. Sci. U.S.A.* **102,** 12612–12617
19. Raboy, V. (2007) The ABCs of low-phytate crops. *Nat. Biotechnol.* **25,** 874–875
20. Shi, J., Wang, H., Wu, Y., Hazebroek, J., Meeley, R. B., and Ertl, D. S. (2003) The maize low phytic acid mutant *lpa2* is caused by mutation in an inositol phosphate kinase gene. *Plant Physiol.* **131,** 507–515
21. González, B., Schell, M. J., Letcher, A. J., Veprintsev, D. B., Irvine, R. F., and Williams, R. L. (2004) Structure of a human inositol 1,4,5-trisphosphate 3-kinase. Substrate binding reveals why it is not a phosphoinositide 3-kinase. *Mol. Cell* **15,** 689–701
22. Miller, G. J., and Hurley, J. H. (2004) Crystal structure of the catalytic core of inositol 1,4,5-trisphosphate 3-kinase. *Mol. Cell* **15,** 703–711
23. Holmes, W., and Jogl, G. (2006) Crystal structure of inositol phosphate multikinase 2 and implications for substrate specificity. *J. Biol. Chem.* **281,** 38109–38116
24. González, B., Baños-Sanz, J. I., Villate, M., Brearley, C. A., and Sanz-Aparicio, J. (2010) Inositol 1,3,4,5,6-pentakisphosphate 2-kinase is a distant IPK member with a singular inositide-binding site for axial 2-OH recognition. *Proc. Natl. Acad. Sci. U.S.A.* **107,** 9608–9613
25. Miller, G. J., Wilson, M. P., Majerus, P. W., and Hurley, J. H. (2005) Specificity determinants in inositol polyphosphate synthesis. Crystal structure of inositol 1,3,4-trisphosphate 5/6-kinase. *Mol. Cell* **18,** 201–212
26. Wang, H., Falck, J. R., Hall, T. M., and Shears, S. B. (2012) Structural basis for an inositol pyrophosphate kinase surmounting phosphate crowding. *Nat. Chem. Biol.* **8,** 111–116
27. Baños-Sanz, J. I., Villate, M., Sanz-Aparicio, J., Brearley, C. A., and González, B. (2010) Crystallization and preliminary x-ray diffraction analysis of inositol 1,3,4,5,6-pentakisphosphate kinase from *Arabidopsis thaliana*. *Acta Crystallogr. Sect. F Struct. Biol. Cryst. Commun.* **66,** 102–106
28. Baños-Sanz, J. I., Sanz-Aparicio, J., Brearley, C. A., and González, B. (2012) Expression, purification, crystallization, and preliminary x-ray diffraction analysis of the apo-form of IP_5-2K from *Arabidopsis thaliana*. *Acta Crystallogr. Sect. F Struct. Biol. Cryst. Commun.* **68,** 701–704
29. Battye, T. G., Kontogiannis, L., Johnson, O., Powell, H. R., and Leslie, A. G. (2011) iMOSFLM. A new graphical interface for diffraction-image processing with MOSFLM. *Acta Crystallogr. D Biol. Crystallogr.* **67,** 271–281
30. Evans, P. (2006) Scaling and assessment of data quality. *Acta Crystallogr. D Biol. Crystallogr.* **62,** 72–82
31. Collaborative Computational Project Number 4 (1994) The CCP4 suite. Programs for protein crystallography. *Acta Crystallogr. D Biol. Crystallogr.*

50, 760–763
32. McCoy, A. J., Grosse-Kunstleve, R. W., Adams, P. D., Winn, M. D., Storoni, L. C., and Read, R. J. (2007) Phaser crystallographic software. *J. Appl. Crystallogr.* **40,** 658–674
33. Murshudov, G. N., Vagin, A. A., and Dodson, E. J. (1997) Refinement of macromolecular structures by the maximum-likelihood method. *Acta Crystallogr. D Biol. Crystallogr.* **53,** 240–255
34. Emsley, P., and Cowtan, K. (2004) Coot. Model-building tools for molecular graphics. *Acta Crystallogr. D Biol. Crystallogr.* **60,** 2126–2132
35. Laskowski, R. A., MacArthur, M. W., Moss, D. S., and Thornton, J. M. (1993) PROCHECK. A program to check the stereochemical quality of protein structures. *J. Appl. Crystallogr.* **26,** 283–291
36. DeLano, W. L. (2002) *The PyMOL Molecular Graphics System.* DeLano Scientific LLc, San Carlos, CA
37. Hayward, S., and Lee, R. A. (2002) Improvements in the analysis of domain motions in proteins from conformational change. DynDom Version 1.50. *J. Mol. Graph. Model.* **21,** 181–183
38. Mayr, G. W., Windhorst, S., and Hillemeier, K. (2005) Antiproliferative plant and synthetic polyphenolics are specific inhibitors of vertebrate inositol-1,4,5-trisphosphate 3-kinases and inositol polyphosphate multikinase. *J. Biol. Chem.* **280,** 13229–13240
39. Rowan, A. S., Nicely, N. I., Cochrane, N., Wlassoff, W. A., Claiborne, A., and Hamilton, C. J. (2009) Nucleoside triphosphate mimicry. A sugar triazolyl nucleoside as an ATP-competitive inhibitor of B. anthracis pantothenate kinase. *Org. Biomol. Chem.* **7,** 4029–4036
40. Gosein, V., Leung, T. F., Krajden, O., and Miller, G. J. (2012) Inositol phosphate-induced stabilization of inositol 1,3,4,5,6-pentakisphosphate 2-kinase and its role in substrate specificity. *Protein Sci.* **21,** 737–742
41. Bossemeyer, D. (1994) The glycine-rich sequence of protein kinases. A multifunctional element. *Trends Biochem. Sci.* **19,** 201–205
42. Taylor, S. S., Radzio-Andzelm, E., Madhusudan, Cheng, X., Ten Eyck, L., and Narayana, N. (1999) Catalytic subunit of cyclic AMP-dependent protein kinase. Structure and dynamics of the active site cleft. *Pharmacol. Ther.* **82,** 133–141
43. Cox, S., Radzio-Andzelm, E., and Taylor, S. S. (1994) Domain movements in protein kinases. *Curr. Opin. Struct. Biol.* **4,** 893–901
44. Abdullah, M., Hughes, P. J., Craxton, A., Gigg, R., Desai, T., Marecek, J. F., Prestwich, G. D., and Shears, S. B. (1992) Purification and characterization of inositol-1,3,4-trisphosphate 5/6-kinase from rat liver using an inositol hexakisphosphate affinity column. *J. Biol. Chem.* **267,** 22340–22345
45. Nalaskowski, M. M., Bertsch, U., Fanick, W., Stockebrand, M. C., Schmale, H., and Mayr, G. W. (2003) Rat inositol 1,4,5-trisphosphate 3-kinase C is enzymatically specialized for basal cellular inositol trisphosphate phosphorylation and shuttles actively between nucleus and cytoplasm. *J. Biol. Chem.* **278,** 19765–19776
46. Voglmaier, S. M., Bembenek, M. E., Kaplin, A. I., Dormán, G., Olszewski, J. D., Prestwich, G. D., and Snyder, S. H. (1996) Purified inositol hexakisphosphate kinase is an ATP synthase. Diphosphoinositol pentakisphosphate as a high energy phosphate donor. *Proc. Natl. Acad. Sci. U.S.A.* **93,** 4305–4310
47. Van Rooijen, L. A., Rossowska, M., and Bazan, N. G. (1985) Inhibition of phosphatidylinositol-4-phosphate kinase by its product phosphatidylinositol 4,5-bisphosphate. *Biochem. Biophys. Res. Commun.* **126,** 150–155
48. Stevenson-Paulik, J., Odom, A. R., and York, J. D. (2002) Molecular and biochemical characterization of two plant inositol polyphosphate 6-/3-/5-kinases. *J. Biol. Chem.* **277,** 42711–42718
49. Xia, H. J., Brearley, C., Elge, S., Kaplan, B., Fromm, H., and Mueller-Roeber, B. (2003) *Arabidopsis* inositol polyphosphate 6-/3-kinase is a nuclear protein that complements a yeast mutant lacking a functional ArgR-Mcm1 transcription complex. *Plant Cell* **15,** 449–463
50. Brearley, C. A., and Hanke, D. E. (1996) Inositol phosphates in the duckweed *Spirodela polyrhiza* L. *Biochem. J.* **314,** 215–225
51. Sweetman, D., Stavridou, I., Johnson, S., Green, P., Caddick, S. E., and Brearley, C. A. (2007) *Arabidopsis thaliana* inositol 1,3,4-trisphosphate 5/6-kinase 4 (*At*ITPK4) is an outlier to a family of ATP-grasp fold proteins from *Arabidopsis*. *FEBS Lett.* **581,** 4165–4171
52. Josefsen, L., Bohn, L., Sørensen, M. B., and Rasmussen, S. K. (2007) Characterization of a multifunctional inositol phosphate kinase from rice and barley belonging to the ATP-grasp superfamily. *Gene* **397,** 114–125
53. Caddick, S. E., Harrison, C. J., Stavridou, I., Mitchell, J. L., Hemmings, A. M., and Brearley, C. A. (2008) A *Solanum tuberosum* inositol phosphate kinase (StITPK1) displaying inositol phosphate-inositol phosphate and inositol phosphate-ADP phosphotransferase activities. *FEBS Lett.* **582,** 1731–1737
54. Hyeon, C., Jennings, P. A., Adams, J. A., and Onuchic, J. N. (2009) Ligand-induced global transitions in the catalytic domain of protein kinase A. *Proc. Natl. Acad. Sci. U.S.A.* **106,** 3023–3028